nature ecology & evolution

Article

https://doi.org/10.1038/s41559-025-02651-5

Genomic and phenotypic evidence support visual and olfactory shifts in primate evolution

Received: 27 August 2023

Accepted: 31 January 2025

Published online: 28 February 2025

Check for updates

Hai Chi[1,18], Jiahui Wan[2,18], Amanda D. Melin[3,4,5,18], Alex R. DeCasien[6], Sufang Wang[2], Yudan Zhang[2], Yimeng Cui[1,7], Xin Guo[1], Le Zhao[1,8], Joseph Williamson[9], Tianmin Zhang[1,2], Qian Li[2], Yue Zhan[1,7], Na Li[1], Jinqu Guo[1], Zhe Xu[1], Wenhui Hou[1], Yumin Cao[1], Jiaqing Yuan[1], Jiangmin Zheng[2], Yong Shao[10], Jinhong Wang[1], Wu Chen[11], Shengjing Song[1], Xiaoli Lu[12], Xiaoguang Qi[13], Guojie Zhang[10,14,15], Stephen J. Rossiter[9], Dong-Dong Wu[10,16,17] ✉, Yang Liu[1] ✉, Huimeng Lu[2] ✉ & Gang Li[1,8] ✉

Sensory trade-offs between vision and olfaction in the evolution and radiation of primates have long been debated. However, insights have been limited by a lack of sensory gene sequences and accompanying functional predictions. Here we conduct large-scale functional analyses of visual and olfactory receptors and related brain regions across extant primates. Our results reveal a visual shift from ultraviolet to violet colour sensitivity in early haplorrhine primates, followed by acceleration in the rhodopsin retinal release rates at the origin of anthropoids, both of which are expected to greatly enhance visual acuity under brighter light conditions. Additionally, we find that the sensitivity of olfactory receptors shifted from narrowly to broadly tuned early in anthropoid evolution. In contrast, strepsirrhines appear to have retained sensitive dim-light vision and underwent functional enhancement of narrowly tuned olfactory receptors. Our models indicate that this would have enhanced odorant discrimination and facilitated olfaction-mediated physiology and behaviour. These differences in tuning patterns of olfactory receptors between major primate lineages mirror well-established morphological differences in external anatomy and brain structures, revealing new mechanisms of olfactory adaptation and evolutionary plasticity. Our multisystem analyses reveal patterns of co-evolution in genomic, molecular and neuroanatomical traits that are consistent with a sensory 'reallocation' rather than strict trade-offs.

The role of evolutionary trade-offs between the visual and olfactory senses during primate evolution has been debated since the earliest descriptions of primates[1]. Early characterizations of anthropoid monkeys and apes focused on visual acuity and colour perception, together with reduced complexity in the morphology of olfactory systems, leading to a persistent narrative that their sense of smell was relatively unimportant[2]. This idea has been challenged in recent years by research showing remarkable sensitivity of monkeys to specific odorants and the role of olfaction in their social and foraging behaviours[3–5]. In contrast, while extant strepsirrhines possess larger and more complex olfactory structures, implying better olfaction[2], they were long considered to be completely or partially colour-blind[6]. However, recent research has revealed complexity and variation in opsin critical site repertoires across species, challenging the simplistic idea that colour vision in this group is uniformly 'poor'[7].

Current knowledge of primate olfactory evolution comes mainly from studies of the identity and repertoire size comparison of olfactory

A full list of affiliations appears at the end of the paper. ✉e-mail: wudongdong@mail.kiz.ac.cn; yliu@snnu.edu.cn; luhuimeng@nwpu.edu.cn; gli@snnu.edu.cn

receptor (OR) loci, a superfamily of genes that underpins odorant recognition[8–12]. Differences among primate taxa suggest adaptive variation; however, functional analyses of primate ORs are lacking, and this—together with a similar lack of phenotypic data on key ancestral photopigments[6,8,11]—has limited a full understanding of adaptive sensory evolution in primates. In particular, it is still debated whether ancestral primates were nocturnal, cathemeral or diurnal or active during liminal periods, according to different types of data (molecular sequence or diel activity) analysed[2,6,13–17].

To shed new light on the dynamics of visual and olfactory evolution in primates, and reveal the changes in perception that have accompanied the radiation of this diverse order of mammals, here we conduct comprehensive functional genomic analyses based on genomes of 50 species from 14 families representing all major primate lineages, including newly published, high-quality genome data from 27 primate species[18]. To this end, we generate new functional data on colour sensitivity and dim-light adaptation for visual pigments, and combine these with the first comprehensive and systematic models of OR tuning in primates. By integrating results with published genetic, sensory and neuroanatomical data (vomeronasal type 1 receptors (V1Rs), cone/rod densities, visual and olfactory brain regions), we examine patterns of correlated evolution.

Results and discussion

Phenotypic assays for visual pigments

Extant primates express up to four visual pigments in their retina, of which the well-studied mid- and long-wavelength-sensitive (MWS (encoded by *OPN1MW*) and LWS (*OPN1LW*)) pigments of cone cells are sensitive to green and red wavelengths, respectively, and contribute to trichromatic colour vision and acuity[2,13,19,20]. The short-wavelength-sensitive type 1 (SWS1 (*OPN1SW*)) cone pigment also contributes to primate colour vision (ultraviolet (UV) or violet) but its functional evolution is still under debate[13,21,22]. The rhodopsin (RH1 (*RHO*)) photopigment in the rod cells is primarily responsible for dim-light vision[23]. Importantly, RH1 and SWS1 have also been linked to mammalian diel activities[22,24–26], but remain understudied. To assess evolutionary transitions in visual function, we determined the spectral tuning of both SWS1 and RH1 pigments from representative extant primate species and resurrected pigments from key ancestors (Supplementary Figs. 1–4 and Source Data Fig. 1 (Data 1)) using in vitro assays. In these pigments, spectral tuning is largely determined by a subset of amino acids at known critical sites[27,28].

We found that the SWS1 pigment of the earliest primate was UV sensitive (λ_{max} (the wavelength of maximum absorption) = 360 nm) (Fig. 1 and Supplementary Fig. 5), indicating little or no change in spectral tuning since the ancestral placental mammal[27], in contrast to previous results from fewer sequences that reported a shift from UV to violet sensitivity at the base of Euarchonta[13]. Since ancestral reconstructions are sensitive to species coverage and tree topology, we repeated protein sequence inference using ten dataset–tree combinations, and found that the residues at critical sites in the ancestral SWS1 were consistent based on maximum a posteriori (MAP) probability estimation (Source Data Fig. 1 (Data 2)).

We also found evidence that early haplorrhine primates underwent amino acid substitutions at three known critical sites: F46I (posterior probabilities (PP) = 1 and 0.61 for F and I, respectively; T52I (PP = 1 and 0.62); and F86L (PP = 0.91 and 0.94) (Supplementary Fig. 1). Of these, site 86—which showed a robust reconstruction—has previously been reported to have a strong impact on spectral tuning[13,27], and is thus likely to explain the observed dramatic shift in spectral sensitivity towards longer wavelengths, from UV to violet (λ_{max} = 400 nm) (Fig. 1 and Supplementary Fig. 5). In contrast, the substitutions at sites 46 and 52 and an unchanged residue at the additional critical site 49, all showed ambiguous or poor reconstructions (Methods), despite being identical across all ten dataset–tree combinations (Supplementary Figs. 1 and 2 and Source Data Fig. 1 (Data 2)). Thus, we addressed ambiguity in their ancestral reconstructions by also expressing single-mutant pigments that contained the residue with the second highest PP (46 V, PP = 0.28; 52 T, PP = 0.2; 49 L, PP = 0.36). These assays revealed a small to moderate impact on spectral tuning ($\Delta\lambda_{max}$ = 1–4 nm) (Supplementary Fig. 5) and do not impact the overall conclusions regarding spectral sensitivity shifts. Finally, for each focal node we also examined the potential impact of variation at non-critical sites across the ten ancestral reconstructions. In each case, we expressed the ancestral protein that showed the most amino acid differences (4–8 residues) at non-critical sites compared to our main reconstruction (dataset 1/topology 1) (Source Data Fig. 1 (Data 1)) and found no or minimal differences in spectral tuning in SWS1 (Supplementary Fig. 5). Overall, therefore, our results for the SWS1 phenotype for early haplorrhines supports a diel shift to a brighter light environment in the Haplorrhini ancestor[21]. Since then, violet-sensitive colour vision has been broadly retained by haplorrhine primates (Fig. 1 and Supplementary Fig. 5).

In contrast to SWS1, we recorded almost no change in the spectral tuning of the RH1 pigment in the early evolution of primates (Supplementary Fig. 6). To obtain further insights into the photopic niches of primates, we also measured the rhodopsin retinal release rates (half-life or $t_{1/2}$) for several ancestral and living taxa. Slow retinal release rates confer more sensitive vision in dim-light environments, and are thus considered to be adaptive in nocturnal taxa[29]. We recorded a $t_{1/2}$ value of 25 min in the earliest primate ancestor (Fig. 1 and Supplementary Fig. 7), representing an ~50% increase relative to the ancestor of placentals (55 min)[24]. Therefore, the ancestral primate might not have been strictly nocturnal. Rather, the data suggest activity in brighter light (mesopic) conditions to some extent, supporting some previous studies[16,17,30]. Consistent with this interpretation, we also obtained a $t_{1/2}$ value of ~30 min in several extant primates that are commonly considered nocturnal, but which are also known to be active in twilight and bright moonlight conditions[31]. A second major increase in retinal release rate ($t_{1/2}$ 27–15 min) was observed at the origin of anthropoid primates (Fig. 1 and Supplementary Fig. 7), implying further adaptation to diurnality. This phenotypic shift may have been caused by two amino acid substitutions at reported critical sites for this phenotype: L290I (PP = 0.78 and 1) and S299A (PP = 0.99 and 1)[32,33] (Supplementary Fig. 3). All residues showed robust reconstructions (PP > 0.8) across all ten datasets, with the exception of L290 in two cases (PP = 0.78 and 0.79; Source Data Fig. 1 (Data 2)).

Reconstructed RH1 pigments of ancestral primates were consistent for all reported important sites for retinal release rates[23,32–35] based on MAP estimates, with the exception of the ancestral strepsirrhine, which showed variation at site 266 (V in four and L in six reconstructions; Source Data Fig. 1 (Data 2)). Despite similar physicochemical properties, these residues are associated with a small shift in retinal release rate in human rhodopsin mutants[23]. We thus expressed the ancestral strepsirrhine variant RH1 with V266L (Supplementary Fig. 7) and recorded a ~6 min shift of retinal release rate towards that of primate ancestor, again supporting no change in diel activity.

The rapid retinal release rate seen in the ancestral anthropoid primate appears to have been retained in most extant species. For example, modern humans—which show near-complete sequence conservation with other catarrhine primates—exhibit a $t_{1/2}$ of 17 min, providing that strong evidence that rapid retinal release in primates is a hallmark of a diurnal niche. At the same time, we find evidence of slower kinetics in nocturnal primates than in diurnal species (P = 0.042) (Fig. 1). Most notably, the slowest values were seen in three distantly related taxa that are active at night (tarsier, slow loris and the anthropoid owl monkey), pointing to convergent evolution. Therefore, we suggest that dim-light adaptation mediated by rhodopsin is likely to have been a key factor contributing to the transition of these taxa to a darker niche. Although slow retinal release rates are also observed in some diurnal species, such as macaques and baboons, the ecological reason is not clear and could be species-specific.

https://doi.org/10.1038/s41559-025-02651-5

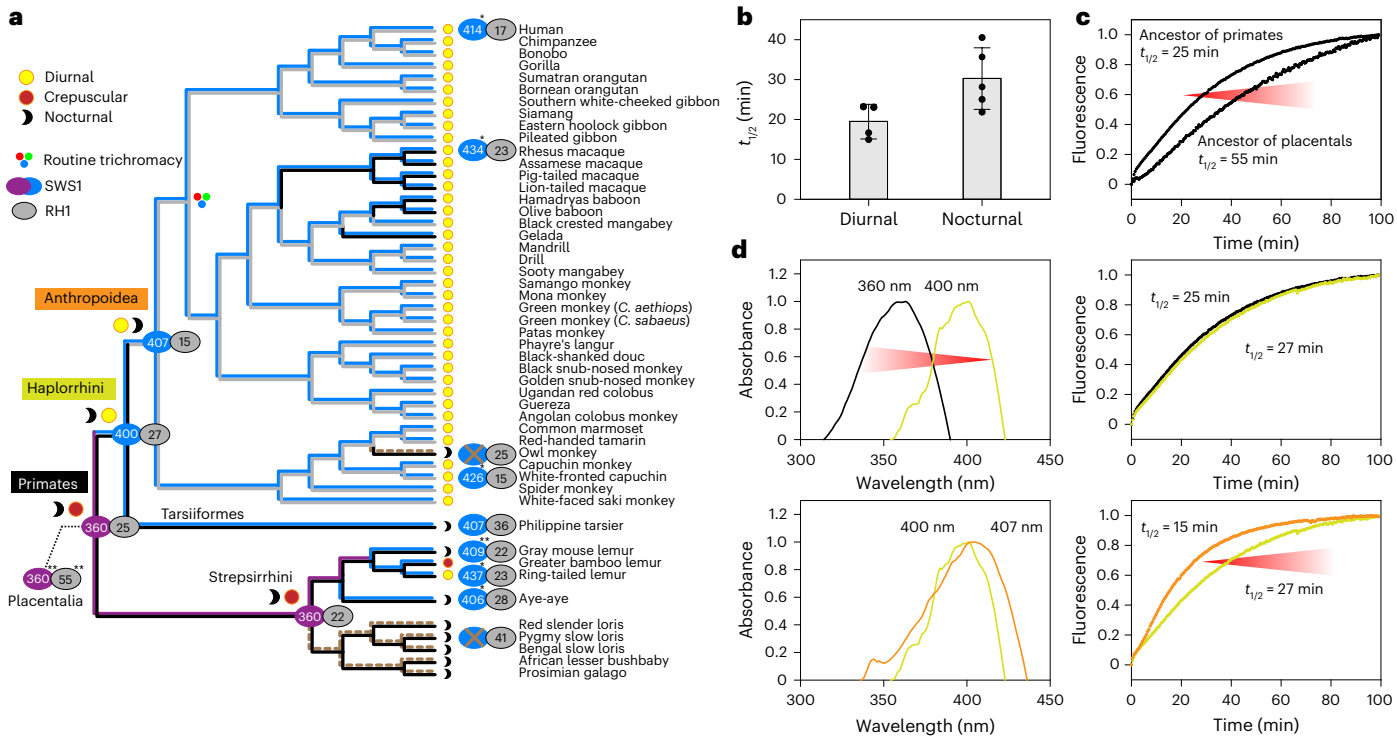

Fig. 1 | Hypotheses of diel activity shifts of early primates based on opsin evidence. a, Functional evolution of SWS1 and RH1 visual pigments mapped onto the primate taxonomic tree[74]. The λ_{max} values of SWS1 pigments are shown in violet (UV sensitive) or blue (violet/blue sensitive). Pseudogenized *SWS1* genes are dashed. For RH1, the half-lives of retinal release rates are mapped, with faster rates shown in grey ($t_{1/2}$ < 20 min) and slower ones in black. The numbers in grey circles are $t_{1/2}$ for each branch. Phenotypic values cited from published literature are indicated by * or ** (based on species from the same genus). **b**, Retinal release rates of rhodopsin from nocturnal primates (30.3 (mean) ± 7.7 (s.d.) min; *n* (number of species) = 5) are significantly slower than diurnal species (19.5 ± 4.3 min; *n* = 4) (P = 0.042, two-tailed *t*-test). The dots are mean values calculated on the basis of three to seven experimental replicates of primate species. **c**, Phenotypic ($t_{1/2}$ of the measured retinal release rate) shift of rhodopsin from primate ancestor compared with placental ancestor. The red arrow shows functional evolution of rhodopsin from the ancestral state. **d**, Two major functional shifts (two red arrows) of both SWS1 and RH1 pigments during the early evolution of primates. The line colours correspond with colours for primate ancestors in **a**.

Our findings indicate that primates underwent marked divergence in photopic niche and visual ecology in their early evolution. Specifically, the ancestral strepsirrhine underwent little functional change from an inferred dim-light (nocturnal and mesopic) active ancestor, whereas changes in photopigment phenotypes imply that the haplorrhines probably experienced two major adaptive transitions to brighter light, which is consistent with evidence based on diel activity data[16,17,31]. In the first of these shifts, we suggest that the violet-shifted spectral tuning of SWS1 pigment at the origin of this clade might have been an adaptation to enhance visual acuity, as well as to avoid UV damage from sunlight[36]. In the second shift, we speculate that the acceleration in rhodopsin kinetics may have allowed early anthropoids to respond more rapidly at light conditions during crepuscular periods[30].

Structural changes of olfactory repertories in primates

To assess whether the detected visual adaptations in primates coincided with evolutionary shifts in olfaction, we conducted a large-scale analysis of *OR* genes. We sought to explore the general patterns and trends in the evolution of olfactory function in primates by analysing structural and functional predictions from tens of thousands of OR proteins. Screens based on molecular docking properties are capable of estimating recognizable odour molecules, including structure-based docking to enrich the most potential active molecules that were previously used[37,38]. We identified and determined the protein structures of 18,051 intact *OR* genes from 50 extant primate species and 7,562 intact *OR* genes from ancestral primate species (Supplementary Fig. 8). We classified ORs into 3,077 functional clusters on the basis of active site dissimilarity and found divergent patterns of evolution across the primate phylogeny (Fig. 2a and Supplementary Figs. 9 and 10).

To interrogate further the phenotypic significance of OR cluster variation, we measured the binding energy of each cluster to a collated set of 2,686 known odorants from experiments[39–42] and assessed their tuning breadths (Supplementary Fig. 9). Our results revealed that OR clusters varied in their binding specificity, with some clusters showing affinity for a broad range of odorants (hereafter referred to as broadly tuned olfactory receptors, BTORs), some showing affinity for a small range of odorants (narrowly tuned olfactory receptors, NTORs) and others showing affinity for an intermediate range (intermediately tuned olfactory receptors, ITORs). We found that the relative abundance of these three forms of OR differed notably between the two main lineages of extant primates (Fig. 2b), with NTORs more abundant in strepsirrhines and BTORs more abundant in anthropoids (Chi-squared test, χ^2 = 677.5, d.f. = 2, P < 0.0001; Fig. 2c), while tarsiers were qualitatively intermediate to both groups. Intriguingly, these shifts in the tuning breadths of ORs correspond to divergence in diel activity as inferred from visual pigments. Specifically, the increase in the numbers of BTORs in the anthropoid primates coincides with their inferred transition to a bright-light niche on the basis of our analyses of visual pigments, whereas the retention and increase in NTOR numbers in the dim-light-adapted strepsirrhines implies that they are better able to detect and discriminate among unique odorants (Supplementary Fig. 11).

Although narrow and broad tuning of ORs has been previously documented[43], little is known about the evolution of such odour-coding systems in mammals and their potential consequences for olfaction.

On the basis of patterns of hierarchical clustering, functional ORs were classified into three groups, based on whether they were present in all primates (clade 1; Supplementary Fig. 10), were lineage-specific (clades 2, 3 and 5–8) or were species-specific (clade 4). ORs that are present across the entire Primates Order suggest strong functional constraint and importance to all primate species. Interestingly, these ORs are more often BTORs. The irregular species-specific OR clusters are more often NTORs (Supplementary Fig. 12; Pearson correlation coefficient 0.1266, $P = 1.8 \times 10^{-12}$), suggesting the presence of new genes and olfactory adaptations for specific odorants at the species level. The remaining clusters show OR loss or presence within specific lineages and indicate that phyletic inertia also plays a role in shaping primate OR composition and diversity.

Further, we found that the presence of BTOR functions showed remarkable consistency with the speciation history of primates, whereas, the tree based on NTOR function showed extensive phylogenetic differences with respect to the primate species tree (Fig. 2d). Odorant recognition depends on the quantitative combinations of activated receptors and is restricted by the odorant concentration[40,43]. This functional interdependence may result in conserved evolution to ensure the capacity of broad olfactory perception. In contrast, NTORs independently respond to odorant stimuli of biological importance, even at very low odorant concentrations[40,43] a situation more likely to induce rapid olfactory differentiation. The different odour-coding model of NTORs to BTORs may reflect and underlie their differing evolutionary dynamics and provide a flexible mechanism for olfactory adaptive evolution.

To obtain further insights into the functional evolution of olfaction in early primates, we assessed changes in odorant recognition of their ORs. For each focal ancestral and extant primate, we derived a measure of the binding energy (potential binding index, PBI) of the complete repertoire of NTORs to each physicochemically defined odorant across 2,686 odorants (Fig. 3a,b). This was repeated for BTORs and ITORs (Supplementary Figs. 13 and 14).

Our analyses indicate that the binding affinity of strepsirrhine ancestor OR repertoires had enhanced binding affinity for, and hence recognition of, aromatics—molecules that are commonly found in glandular secretions and excretions used during scent marking[44,45]. Olfactory communication via long-lasting chemical signals may provide adaptive benefits to nocturnal and solitary primates[44,46]. To compare how ancestral and extant primates vary in the extent to which their ORs show recognition for odorants relevant to scent marking, we collated all volatiles reported to occur in primate glands, faeces and urine. As predicted, the results support high intensity in the average binding energy in the common primate ancestor and early strepsirrhines, but relatively low intensity in anthropoid lineages, adding further support to the hypothesis that early strepsirrhine ancestors relied heavily on olfaction for social communication (Fig. 3c). We repeated these analyses with BTORs and found that, compared to strepsirrhines, haplorrhine receptors show an enhanced trend of binding to esters (Fig. 3d)—molecules that include common plant volatiles[47]. Among ancestral primates, the highest trend of BTOR binding energy for esters was observed at the origin of catarrhines (Supplementary Fig. 13), which is consistent with the appearance of full trichromatic vision and suggests a role in foraging[48,49]. Together our results provide support that emergence of divergent diel niches and foraging ecologies involved the nuanced co-evolution of visual and olfactory sensory systems.

Evolution of brain regions involved in sensory perception

To better understand how sensory-related genotypes and phenotypes co-evolve with brain regions that facilitate sensory perception, we combined our results (number and proportions of N/I/BTORs, retinal release rates of RH1, λ_{max} of RH1 and λ_{max} of SWS1) with species-average published data on: (1) the numbers of functional *V1R* genes (which encode pheromone receptors in the vomeronasal organ (VNO)); (2) densities of visual photoreceptors (rods and cones); (3) overall brain size; and (4) the sizes of brain areas involved in sensory perception (visual areas—primary visual cortex (V1), optic tract, lateral geniculate nucleus of the thalamus (LGN); olfactory areas—accessory and main olfactory bulbs (AOB and MOBs)); and (5) numbers of neurons within and the volumes of two functional layers within the LGN (magnocellular—movement detection; parvocellular—fine detail and colour). For each of the brain regions, we examined both absolute sizes and relative (to overall brain) sizes. We first estimated pairwise phylogenetic correlations between all variables, and then linked specific sensory-related genotypes and phenotypes to brain structure variation across primate species using phylogenetic least-squares regression (PGLS) modelling.

We found that traits were positively correlated within either the visual or olfactory systems, while they tended to be negatively correlated across the sensory modalities (Fig. 4a and Source Data Fig. 4), supporting hypotheses of sensory 'reallocation' in primates. While previous work has demonstrated these patterns among brain regions[50–53], we show that these trade-offs extend to sensory phenotypes and genotypes. Specifically, we find that violet colour sensitivity, retinal release rates, cone densities and visual brain areas were expanded in diurnal species and haplorrhines (Fig. 4a and Source Data Fig. 4). Haplorrhines exhibit a suite of co-evolved adaptations that facilitate visual acuity, including increased orbital convergence[54], which is also positively correlated with the relative size of visual brain areas and number of parvocellular (but not magnocellular) neurons across species[53]. Furthermore, the parvocellular layers are thicker and subdivided into clear sublayers in diurnal primates, while those of nocturnal strepsirrhines are thin and undivided[55]. Although it is likely that the precursors to both magnocellular and parvocellular neurons were present in the earliest primates, the primate LGN distinctly exhibits complete segregation of the cell classes into layers[56]. Strepsirrhines may have experienced an expansion of the olfactory bulbs[57], further supporting their nocturnal niche. This is in line with our findings that rod densities, olfactory gene repertoire sizes and olfactory brain areas were expanded in nocturnal species and strepsirrhines (Fig. 4a, Supplementary Fig. 8 and Source Data Fig. 4).

Regression analyses highlight more precise relationships, particularly within the different olfactory systems. The best-fit models of the AOB suggest that relative AOB size was larger in strepsirrhines, increased with the number of *V1R* genes and with the number or proportion of NTORs and decreased with the proportion of BTORs (Figs. 2c and 4b and Source Data Fig. 4). Relative MOB size was larger in strepsirrhines and increased with the number of NTORs, BTORs and ITORs, with an interaction between sensory traits and suborder (Figs. 2c and 4b and Source Data Fig. 4). These findings are likely to reflect the linked emergence of routine trichromacy and loss of the VNO in catarrhine primates, the latter of which probably drove the loss of the AOB and related OR genes[11,58]. Consistent with this, previous work has shown that relative VNO length predicts the proportion of intact *V1R* genes, while the size of the main olfactory epithelium predicts the total number of *OR* genes[59]. The routinely trichromatic platyrrhine lineage (howler monkeys) exhibited some olfactory gene loss but maintained their VNOs and AOBs[58,60]. Our results also highlight the distinct roles of the AOB (versus the MOB) in processing olfactory information from the VNO[61] and of NTORs (versus BTORs) in perceiving animal-associated biological signals[40], which are supported by previous findings that AOB (versus MOB) size varies across primate mating systems[52,53]. Interestingly, AOB loss in catarrhines suggests a reorganization of social olfactory information processing, bolstering previous claims that a functional VNO is not necessary for semiochemical communication[62–64]. In fact, gibbons (*Hylobates*) and marmosets (*Callithrix*)—both of which possess scent glands and participate in scent marking[65,66]—exhibited the highest NTOR proportions among the anthropoids in our dataset.

We also found that absolute V1 size increased with cone peak density and as half-life of RH1 retinal release decreased (Fig. 4b and Source Data

https://doi.org/10.1038/s41559-025-02651-5

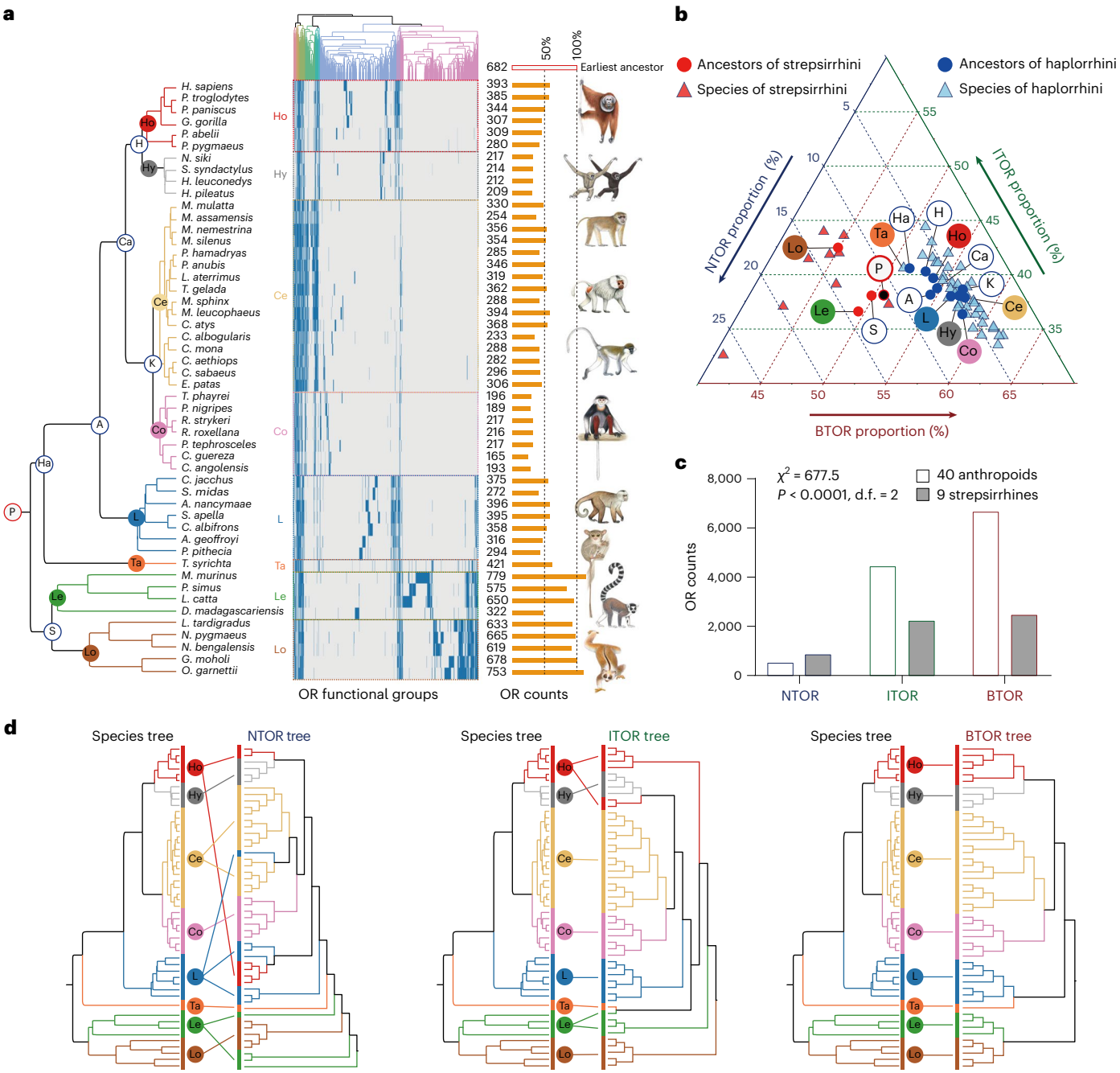

Fig. 2 | Divergent evolution of differently tuned ORs. a, Phylogenetic tree of primates (left), functional OR clustering results (middle) and OR quantities of living and ancestral primate species (right). The dotted line represents the quantity (percentage) of functional ORs relative to the primate ancestor. P, Primates; Ha, Haplorrhini; A, Anthropoidea; Ca, Catarrhini; K, Cercopithecidae; H, Hominoidea; Ho, Hominidae; Hy, Hylobatidae; Ce, Cercopithecinae; Co, Colobinae; L, Platyrrhine; Ta, Tarsiidae; S, Strepsirrhini; Le, Lemuroidea; Lo, Lorisoidea. In the heatmap, each row corresponds to a species (or ancestor), while each column represents one of the 3,077 functional clusters, blue bars denote the presence of different OR functional clusters in the species, while grey bars signify absence. **b**, Ternary plot of the proportion of the three functional groups of OR tuning for ancestral and extant primates. The blue and red triangles refer to the 50 extant species of Haplorrhini and Strepsirrhini in the evolutionary tree of **a** and the blue and red dots refer to the ancestral nodes of primates, denoted by the 15 circularly labelled abbreviated letters in **a**. **c**, Total numbers of differently tuned ORs in early ancestors of anthropoids and strepsirrhines revealing notable differences between ancestors of strepsirrhines and anthropoids. **d**, Topology comparison of the primate species tree (left) and the cluster detection of separated groups of ORs with varied tuned breadth (right). The different lineages of primate are indicated with different colours. Credit: Primate illustrations reproduced with permission from ref. 18, AAAS.

Fig. 4), consistent with faster rhodopsin retinal release rates and the role of cones in colour vision under lit conditions[24,36]. Results were similar for the optic tract and LGN (Source Data Fig. 4), which is consistent with the co-evolution of V1, optic tract and LGN size in primates[50,52]. Overall, our findings suggest that instead of a strict trade-off, the co-evolution of visual and olfactory senses in primates is better explained by sensory reallocation, which is likely to reflect lineage-specific evolutionary shifts in activity period, diet and mating systems[50–53,61,67].

By combining new genomic data with protein modelling, functional assays of visual and olfactory phenotypes and analyses of

https://doi.org/10.1038/s41559-025-02651-5

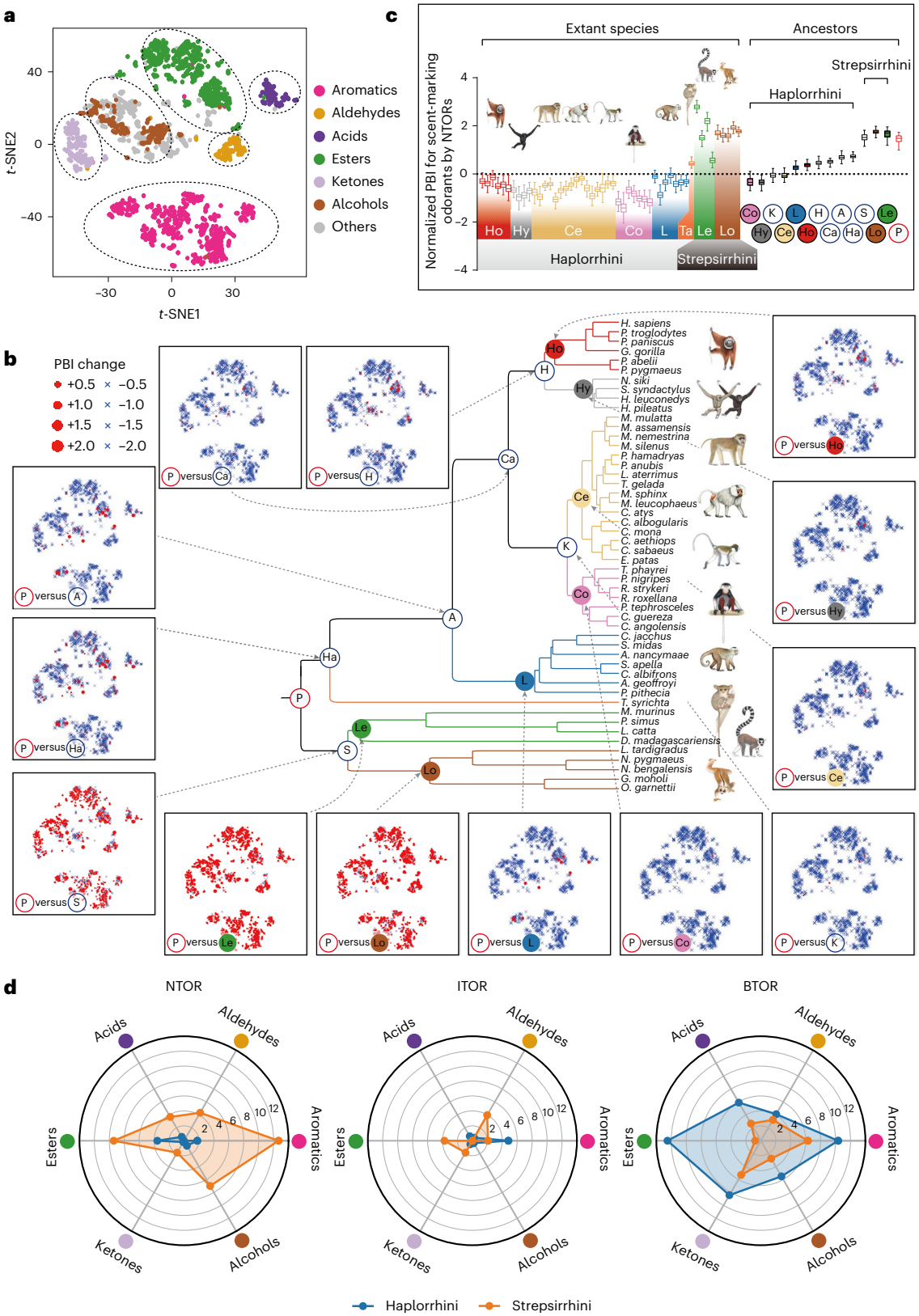

Fig. 3 | Variation of the speculated odorant recognition code by NTORs in primate evolution. a, The *t*-SNE subplot showing the odorant space based on physicochemical descriptors. A total of 2,686 odorants were projected onto a two-dimensional space made of the *t*-SNE dimensionality reduction, with molecular types labelled with different colours. **b**, Comparison of odorant recognition coded by NTORs in key primate ancestors. Taxonomic abbreviations follow those in Fig. 2. Increases and decreases in odorant recognition (PBI) among primate ancestors are shown as red circles and blue crosses, respectively, with intensity represented by symbol size. **c**, Normalized PBIs for scent-marking odorants in extant and ancestral primates as calculated from their NTOR-binding energies. **d**, Comparison of olfactory functional binding enhancements. Radar charts suggest olfactory functional binding enhancement of haplorrhine (blue) and strepsirrhine (red) ancestors to six odorant types (aromatics, aldehydes, acids, esters, ketones and alcohols). Numbers on the circles are the average enhancement scores. Credit: Primate illustrations reproduced with permission from ref. 18, AAAS.

https://doi.org/10.1038/s41559-025-02651-5

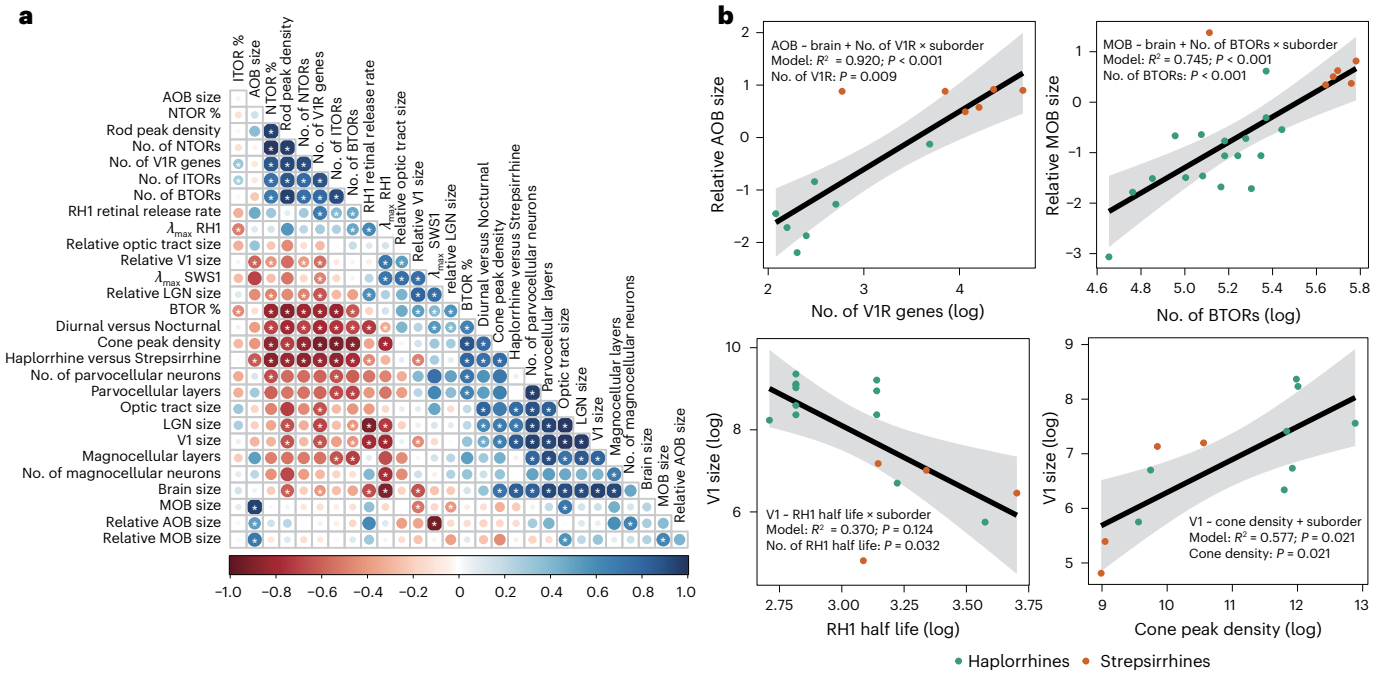

Fig. 4 | Co-evolution between visual and olfactory genotypes and phenotypes and neuroanatomical traits. a, Phylogenetic correlations (*r* values) between all variables analysed here. Blue, positive; red, negative; * indicates a significant (two-sided nominal $P < 0.05$) correlation (correlations and exact *P* values are provided in the Source Data). **b**, Relationships between select visual and olfactory traits. Ordinary least-squares regression lines are shown in black, with confidence intervals in grey. Each dot represents the average value for one species. Model details (R^2 values and nominal *P* values) are provided for each plot.

perceptual brain areas, we provide insights into the evolution and diversification of primates and their sensory systems. Notably, we show that sensory trait co-evolution can be detected across biological levels, spanning genomic, molecular and neuroanatomical traits. While kinetic analyses of reconstructed ancestral visual pigments indicate that the earliest primates were active in dim light rather than strictly very dark, scotopic niches, we find that the subsequent emergence of predominantly dim-light and bright-light active lineages coincided with evolutionary expansions of olfactory and visual capabilities, respectively. Our analyses of *OR* and *V1R* genes also reveal somewhat independent evolution of the different olfactory systems, in line with their established roles in processing different types of olfactory information. Furthermore, shifts in OR repertoire structure and modelled function, including expansion of NTORs and BTORs in strepsirrhines and anthropoids, respectively, may have important implications for brain evolution. For example, it has been suggested that NTORs elicit hardwired physiological or behavioural responses[40], whereas BTORs are linked to learned behaviours[68]. This scenario is consistent with expansion of cortical association areas, which integrate sensory inputs and facilitate learning, in anthropoids relative to strepsirrhines[69]. The results presented here, combined with previous studies of primate socioecological variation, highlight the complex interplay between and importance of both sensory modalities across primate lineages and provide new insight and areas for thought regarding the adaptive origins and evolution of primates.

Methods

Genome data

We used a newly published dataset of long-read, high-coverage genomes from the primate genomes project[18,70], along with previously published reference genomes of primates (Supplementary Table 1). Altogether, the genomes of 50 species from 14 families representing all major primate lineages were analysed, which are shown in the Supplementary Table 1.

Primate opsin sequence acquisition

For *RH1*, we combined 89 published sequences from both GenBank (www.ncbi.nlm.nih.gov/genbank) and an unpublished sequence of *Nycticebus pygmaeus*[70]. For *SWS1*, 107 gene-coding sequences were obtained from the public database and the unpublished genome of *N. pygmaeus*[70]. We also obtained both gene sequences from species across nine other mammalian Orders as outgroups (Supplementary Table 2).

Ancestral sequence reconstruction for primate opsins

Coding sequences of *RH1* and *SWS1* orthologues were aligned separately using ClustalW (MEGA X)[71]. Given that ancestral sequence reconstruction will be affected by both representative sequences and tree topology used, we carried out multiple inferences to test the robustness of our conclusions. In total, five datasets were used for each of the opsin genes: dataset 1, SWS1 and RH1 (50 primates and 18 outgroups); dataset 2 (expanded both primate and outgroup species), SWS1 (107 primates and 42 outgroups) and RH1 (89 primates and 43 outgroups); dataset 3 (expanded outgroups), SWS1 (50 primates and 42 outgroups) and RH1 (50 primates and 43 outgroups); dataset 4 (one representative species from each genus according to dataset 1), SWS1 and RH1 (38 primates and 18 outgroups); and dataset 5 (one representative species from each genus according to dataset 2), SWS1 (53 primates and 39 outgroups) and RH1 (49 primates and 39 outgroups). For inactivated *SWS1* genes, indels or premature stop codons were removed before the ancestral sequence reconstructions. We used ProtTest 3 (ref. 72) to calculate the best-fitting model of amino acid evolution for RH1 as LG + I + G (datasets 1 and 3–5) or LG + G (dataset 2) and for SWS1 as JTT + G (datasets 1–5). Ancestral sequences of both opsins were inferred using Codeml (PAML 4 package)[73], based on two species tree topologies that differ with respect to the placement of outgroups[74–76] (Source Data Fig. 1 (Data 3)). RH1 sequences of extant taxa were the same length. SWS1 sequences of extant taxa contained indels (see alignment, Source Data Fig. 1 (Data 4)); however, these were absent from ancestral sequences based on parsimony-based reconstruction in Mesquite 3 (ref. 77). All

ancestral sequences reconstructed by different datasets and topologies are listed in Source Data Fig. 1 (Data 1), with the length of either SWS1 or RH1 the same across focal ancestors. Ancestral sequence reconstructions with residue posterior probabilities are shown in Source Data Fig. 1 (Data 2). Reconstructions are coded as robust (MAP > 0.8); ambiguous (MAP < 0.8, second highest PP > 0.2); or poor (MAP < 0.8, second highest PP < 0.2)[78].

In vitro functional assay for primate visual pigments

Representative *RH1* and *SWS1* sequences from extant primate species and their ancestors were synthesized in vitro and then subcloned into pcDNA3.1 (+) expression vector (Invitrogen), with a Kozak sequence (CCACC) (5′ end) and a 1D4 tag (ACA GAG ACC AGC CAA GTG GCG CCT GCC) (3′ end), respectively. By using Xfect reagent (Clontech, catalogue no. 631317), the plasmid containing opsin-coding sequence was transfected into HEK293T cells, which were then collected after a 48 h transfection. Subsequently, by incubating the cells together with 11-*cis*-retinal (at 4 °C), visual pigment was regenerated and then purified by monoclonal antibody (Rho 1D4, University of British Columbia). A spectral sensitivity curve was able to be recorded for each visual pigment after successful expression and purification[21,79,80]. For primate SWS1 pigment, the spectral sensitivity (the wavelength of maximum absorption, λ_{max}) was first measured by a U-3900 spectrophotometer (Hitachi) in the dark and then measured again after either H_2SO_4 treatment or light bleaching. For primate RH1, the spectral sensitivity was also measured by the spectrophotometer. Additionally, the retinal release rate of RH1 was measured by a Cary Eclipse fluorescence spectrophotometer (Agilent) under condition of 20 °C, following published literature for details of experimental procedures[24,80]. Measured data were fitted by $y=y_0+a(1-e^{-bx})$, with the half-life value calculated from $t_{1/2}=\ln 2/b$ (Source Data Fig. 1 (Data 5)). We also generated SWS1 single mutants with alternative residue states based on reconstructed ancestors of Haplorrhini (I46 V, F49 L and I52 T) and Anthropoidea (L52 F). For these, polymerase chain reaction studies were conducted using FastPfu DNA polymerase (TransGen Biotech, catalogue no. AP221-01) and amplified plasmids were digested using DpnI (New England Biolabs, catalogue no. R0176V). After verification by sequencing, mutants were then transfected and functionally measured as described procedures. We tested for correlations between our newly measured phenotypic data from visual pigments with published cone and rod peak densities from primate species (Supplementary Table 3). These photoreceptor densities provide an independent assessment of the energy allocation into different types (acute, colour vision under bright light (cones), versus sensitivity and motion detection in dim light (rods)) of vision.

Identification of ORs and OGGs

We applied an established pipeline to identify all intact and pseudogenized *OR* genes present in the 50 primate genomes[81]. To trace the evolution of primate ORs, we classified retrieved *OR* genes into primate OR orthologous gene groups (OGGs) following published methods[11,82] (Supplementary Methods).

Structure-based OR–odorant pairs dataset construction

The pipelines used for the structure-based OR–odorant pairs dataset construction are summarized as Supplementary Fig. 9a. For OR structure preparation, given that the study was conducted before the public release of the AlphaFold2 (AF2) software, we initially built the OR structures using I-TASSER[83] and further refined them using all-atom molecular dynamics under a mimic physiological environment with NAMD (v.3.0a)[84] and CHARMM36m[85] force field. The simulation temperature was set to 310 K and the pressure was maintained at 1 atm. The stable structures after final 50-ns MD simulations at NPT ensemble were collected for molecular docking. The endogenous binding sites of ORs were predicted with COACH[86]. We have additionally reperformed the protein structure modelling of all primate ancestral ORs using AF2 software. The results show that the molecular docking values are substantially correlated between AF2 and our I-TASSER with MD structures. Considering the important role of MD in optimizing the structural rationality of proteins[87], the strategy of I-TASSER with MD was used in this paper to complete all the analyses.

To validate the accuracy of our modelled structure, we used a combination of I-TASSER with MD to generate a three-dimensional model of the OR51E2 protein structure, which stands as the sole OR with a published cryo-electron microscopy (cryo-EM) structure[88]. The modelling process was conducted thrice and our calculated models were compared against the cryo-EM structure. Test results reveal a root-mean-square deviation (RMSD) value of ~3.5 Å between our calculated model and the cryo-EM structure, with residue alignment within a 20-Å radius around the core region of the protein averaging at ~2 Å.

In accordance with suggestions from previously published research[89], wherein a protein alignment RMSD result of 4 Å and a transmembrane region RMSD of 2.5 Å were deemed indicative of structural proximity to the original, our comparison yielded RMSD values below this threshold. This outcome underscores the reliability of our modelling approach used in this study. Given the tremendous members of OR proteins, that were predicted structures in this work, they were not directly tested experimentally.

For odorant data collection, we mined 2,686 odorant molecules from published sources[36–39]. Molecular structures and physicochemical descriptors of odorants were obtained from PubChem (https://pubchem.ncbi.nlm.nih.gov)[90] and OCHEM (https://ochem.eu)[91], respectively. To model the physicochemical space of selected odorants, the functional group descriptors based on SMILES format of odorants[92] and other 32 optimized key physicochemical descriptors (for example, molecular weight, carbon chain length, logP and so on; Source Data Fig. 3 (Data 1 and 2))[93] were normalized to conduct *t*-distributed stochastic neighbour embedding (*t*-SNE) analysis[94]. Odorants were classified into six types: aromatics, aldehydes, acids, esters, ketones and alcohols on the basis of their physicochemical characters.

We performed flexible molecular docking for OR–odorant pairs with AutoDock Vina[95] for representative ORs from 682 OGGs, observed in the most recent common ancestor (MRCA) of primates. The binding modes of a 682 × 2,686 OGG OR–odorant pairs dataset were collected to conduct active site identification for clustering the functional OR groups. Therefore, 3,077 functional OR groups were clustered on the basis of active site similarity.

Next, the docking scores of the representative 3,077 × 2,686 OR–odorant pairs dataset were ascertained using Vina. There is a positive correlation between the experiment-activated hits and absolute-affinity scores in the docking screening process[37,38], thus the ORs with higher absolute affinity to much odorants scores have the notable trend to recognize more odorants, which are considered as BTORs.

The potential binding combinations between odorant datasets and structures of all functional OR clusters were visualized as a heatmap using the Heatmaply package[96] in R (v.4.03). On the basis of the descriptive statistics of agonist spectra from the ORs and odorants binding combinations, ORs were classified into three groups following two steps. First, the lower outliers in the OR binding distribution was determined by the ORs and odorants binding distribution based on

$$x < [\text{lower quartile} - 1.5 \times (\text{upper quartile} - \text{lower quartile})],$$

in which x is the binding odorant counts of each OR, lower quartile and upper quartile are 25th and 75th percentiles of the distribution of ORs and odorants binding combinations.

Initially, the number of odorants with potential binding ability for each OR functional cluster is calculated. Subsequently, a box-and-whisker plot is constructed on the basis of these numbers. The upper quartile and lower quartile delineate the box boundaries and OR clusters exceeding these boundaries by 1.5 times the range of

the box are identified as outliers. Upon observing the box-and-whisker plot, it is noted that ~11.58% of the ORs fall within the lower outlier range (binding odorant counts <1,012), while upper outliers are absent. Consequently, ORs within the lower outlier range are classified as NTORs. However, as there were no upper outliers in the quantitative distribution plot of OR affinity, the upper outlier scheme was not used for delineating BTORs. Instead, the median (binding odorant count is 2,041) of the remaining data after dividing NTORs was used as the boundary between BTORs and ITORs.

Hierarchical clustering of differently tuned ORs was established on the basis of their Euclidean distance (Fig. 2a and Supplementary Fig. 10) and compared with the primate species tree (Fig. 2d). Specifically, we used the program Heatmaply package in R (v.4.03) to conduct the hierarchical cluster analysis based on the distribution of the 3,077 OR functional clusters across different species (or ancestors). Adjacent branches signify similar distribution patterns of these OR functional clusters across different species (including ancestors). Consequently, the eight clades depicted in the tree (top, Supplementary Fig. 10) delineate three broad distribution patterns of OR functional clusters. The clustering process entailed: (1) computing the distance between pairs of functional clusters based on the occurrence data of the 3,077 functional clusters among species (including ancestors) using the Euclidean distance algorithm, (2) using the complete-linkage algorithm to perform hierarchical clustering of functional clusters based on the distance matrix, where clusters with the closest distances from neighbouring branches of the tree and this process iterates layer by layer, and (3) displaying the clustering results in the form of a tree atop the heatmap.

Functional ORs clustering based on active site similarity

The residues involved in receptor–ligand interaction in 682 × 2,686 OGG OR–odorant pairs dataset were identified by hydrogen-bond formation and native contact analysis (cutoff set as 3.6 Å) with PyMOL (v.2.3.0)[97]. To further identify the active sites, we used Z score to estimate the contribution for each residue involved in odorant recognition, calculated by

$$Z\,\mathrm{score}_i = \frac{N_i - \bar{N}}{\sqrt{\frac{1}{A-1}\sum (N_i - \bar{N})^2}},$$

in which i is the residue position in the aligned OR sequences, N_i is the number of odorant molecules interacting with ith residue in all OR–odorant pairs, $\bar{N}$ is the average number of odorant molecules interacting with each residue and A represents the total residue number in the normalized OR sequence. The 26 residues with higher interaction contribution (>95% upper confidence interval or $Z > 1.64$) were used as active sites for functional OR clustering. We used the software CD-HIT[98] to recluster all 25,614 ORs into 3,077 clusters on the basis of the dissimilarities of their active sites (tolerance 5%), which have the dominant influence to the odorant recognition of ORs[99].

Evaluating the consistency of the odorant recognition

We acquired the human ORs and the relative odorants which have been experimentally tested previously[39] to rerun our pipeline to evaluate the consistency of the odorant recognition of ORs given by the current developed computational methods and the experiment tests (Supplementary Methods).

Estimating the changes of odorant recognition

To estimate the changes of odorant recognition among primate early ancestors, we calculated the PBI, that measures both docking score and presumed active OR numbers[100], to test the ability of odorants recognition between OR repertoires and odorants. For each odorant in the 3,077 × 2,686 OR–odorant pairs dataset, proposed

$$\mathrm{PBI} = \log(|S_{\min}| + 1) \times \log(M + 1),$$

where $S_{\min}$ is the smallest docking score of OR–odorant pairs in a primate lineage and M is the number of ORs in the primate lineage with a docking score lower than −4.5, to filter out the noises of OR binding with low probabilities (Supplementary Fig. 9c)[42]. A higher PBI is indicative of a primate lineage with a stronger odorant recognition ability, while a lower PBI indicates the opposite. Thus, a PBI difference between two ancestors can be indicative of functional enhancement (positive PBI difference) or attenuation (negative PBI difference) for a given odorant (Fig. 3b and Supplementary Figs. 13 and 14).

We used the Chi-square goodness-of-fit test to assess whether there was a shift in the distribution of tuned OR repertories following the extant species of strepsirrhines and anthropoids, based on the counts of NTORs, ITORs and BTORs in the two species groups. The correlation between the binding percentage for odorant dataset and covering percentage conserved in living species of functional OR clusters was statistically calculated by Pearson correlation index, to show the relationship of the functional conservation and tuning breadth of primate ORs (Supplementary Fig. 12). The relationship between OR pocket size and affinity-score value was also checked by Pearson correlation test (Supplementary Fig. 9d).

We used T score to normalize the PBI values to identify the significantly increased binding ability of each primate ancestor to specific odorant.

$$T\,\mathrm{score}_{(i,j)} = \frac{\mathrm{PBI}_{(i,j)} - \mathrm{PBI}_{(\mathrm{node}\,P,j)}}{\sqrt{\frac{1}{n-1}\sum (\mathrm{PBI}_{(i,j)} - \overline{\mathrm{PBI}}_{(\,j)})^2}},$$

in which i is the node index of primate ancestors and j is the index of an odorant, $\mathrm{PBI}_{(i,j)}$ is the calculated PBI value of primate ancestor node i to odorant j, $\mathrm{PBI}_{(\mathrm{node}\,P,j)}$ is the calculated PBI value of the MRCA of primate to odorant j, $\overline{\mathrm{PBI}}_{(\,j)}$ is the average PBI value of all studied primate ancestors to odorant j and n represents the number of all studied primate ancestor nodes.

Significant values of $\mathrm{PBI}_{(i,j)}$ ($\mathrm{PBI}_{(i,j)}$ > upper 95% CI of t-distribution or T score > 1.77, d.f. = 13) were characterized as the significantly enhanced PBI of the primate ancestor node i of odorant j compared to $\mathrm{PBI}_{(\mathrm{node}\,P,j)}$. The T scores of significantly enhanced PBIs of each primate ancestor to the same typed odorant (aromatics, aldehydes, acids, esters, ketones and alcohols) were summed to give an overall olfactory functional enhancement value of each primate ancestor to the independent typed odorants. We then calculated the average enhancement score of all haplorrhine and strepsirrhine ancestors to each odorant type, respectively, to show the olfactory functional divergence between these two major primate lineages (Fig. 4a).

Brain analyses

We collected neuroanatomical traits from published literature sources, including the volumes of the whole brain, MOB, AOB, V1 grey matter, optic tract and LGN[101] and the volumes and numbers of neurons within the magnocellular and parvocellular layers of the LGN[50] (Source Data Fig. 4). Sensory genotypes and phenotypes were obtained from the current study (count and proportion of NTORs/ITORs/BTORs; λ_{max} of SWS1, λ_{max} of RH1; RH1 half-life) and from published literature sources (count of *V1R* genes; cone and rod peak density)[102] (Source Data Fig. 4 and Supplementary Table 3).

We estimated the phylogenetic correlation (covariance) between all pairs of neuroanatomical and sensory variables (using the phyl.vcv function in the R package phytools)[101,103] and then scaled the covariance matrix into the corresponding correlation matrix (using the cov2cor function in the R package stats). T statistics were estimated using the following equation: $t = r \times \sqrt{((N-2)/(1-r^2))}$. Two-tailed P values were derived from the t-distribution (with degrees of freedom equal to the number of species minus 2) (Source Data Fig. 4). Correlations were visualized using the corrplot R package and ordered according to the

angular order of the eigenvectors. Relative brain region sizes were estimated as the residuals from PGLS regression models of each region (log-transformed) as a function of brain size (both log-transformed) and suborder (using the comparative.data and pgls functions in the R package caper)[104]. Lambda was allowed to take its maximum likelihood value and we used the 10kTrees consensus phylogeny[105].

We also used PGLS regression models to investigate relationships between specific neuroanatomical traits and sensory genotypes/phenotypes, since these models allow us to account for evolutionary relationships between species. For each unique combination of visual or olfactory neuroanatomical traits and visual or olfactory sensory genotypes/phenotypes (for example, AOB volume and number of *V1R* genes; LGN volume and cone peak density), we tested whether the sensory traits predicted the neuroanatomical traits (absolute or relative to brain size) by running four PGLS models.

The absolute models were as folllows:

- log(neuroanatomical trait) ~ log(sensory genotype/phenotype) + suborder
- log(neuroanatomical trait) ~ log(sensory genotype/phenotype) + suborder + log(sensory genotype/phenotype) × suborder

The relative models were as follows:

- log(neuroanatomical trait) ~ log(brain size) + log(sensory genotype/phenotype) + suborder
- log(neuroanatomical trait) ~ log(brain size) + log(sensory genotype/phenotype) + suborder + log(sensory genotype/phenotype) × suborder

Lambda was allowed to take its maximum likelihood value and we used the 10kTrees consensus phylogeny[105]. Model fits were compared using the Bayesian information criterion (BIC) (using the BIC function in the R package stats) and coefficient estimates and *P* values were extracted from the models (Source Data Fig. 4).

Reporting summary

Further information on research design is available in the Nature Portfolio Reporting Summary linked to this article.

Data availability

All sequence and phenotypic data are listed in the text and Supplementary Information. Source data are provided with this paper.

Code availability

Code to run the analyses is available at https://github.com/GanglabSnnu/OR_identify.

References

1. Clark, W. E. L. G. *The Antecedents of Man: An Introduction to the Evolution of the Primates* (Harper, 1963).
2. Kawamura, S. & Melin, A. D. in *Evolution of the Human Genome I: The Genome and Genes* (ed. Saitou, N.) 181–216 (Springer, 2017).
3. Shepherd, G. M. The human sense of smell: are we better than we think? *PLoS Biol.* **2**, E146 (2004).
4. Charpentier, M. J., Mboumba, S., Ditsoga, C. & Drea, C. M. Nasopalatine ducts and flehmen behavior in the mandrill: reevaluating olfactory communication in Old World primates. *Am. J. Primatol.* **75**, 703–714 (2013).
5. Heymann, E. W. The neglected sense-olfaction in primate behavior, ecology, and evolution. *Am. J. Primatol.* **68**, 519–524 (2006).
6. Tan, Y., Yoder, A. D., Yamashita, N. & Li, W. H. Evidence from opsin genes rejects nocturnality in ancestral primates. *Proc. Natl Acad. Sci. USA* **102**, 14712–14716 (2005).
7. Jacobs, R. L. et al. Novel opsin gene variation in large-bodied, diurnal lemurs. *Biol. Lett.* **13**, 20170050 (2017).
8. Nei, M., Niimura, Y. & Nozawa, M. The evolution of animal chemosensory receptor gene repertoires: roles of chance and necessity. *Nat. Rev. Genet.* **9**, 951–963 (2008).
9. Matsui, A., Go, Y. & Niimura, Y. Degeneration of olfactory receptor gene repertories in primates: no direct link to full trichromatic vision. *Mol. Biol. Evol.* **27**, 1192–1200 (2010).
10. Mombaerts, P. Genes and ligands for odorant, vomeronasal and taste receptors. *Nat. Rev. Neurosci.* **5**, 263–278 (2004).
11. Niimura, Y., Matsui, A. & Touhara, K. Acceleration of olfactory receptor gene loss in primate evolution: possible link to anatomical change in sensory systems and dietary transition. *Mol. Biol. Evol.* **35**, 1437–1450 (2018).
12. Niimura, Y. & Nei, M. Evolution of olfactory receptor genes in the human genome. *Proc. Natl Acad. Sci. USA* **100**, 12235–12240 (2003).
13. Melin, A. D. et al. Euarchontan opsin variation brings new focus to primate origins. *Mol. Biol. Evol.* **33**, 1029–1041 (2016).
14. Griffin, R. H., Matthews, L. J. & Nunn, C. L. Evolutionary disequilibrium and activity period in primates: a Bayesian phylogenetic approach. *Am. J. Phys. Anthropol.* **147**, 409–416 (2012).
15. Wu, Y., Wang, H., Wang, H. & Hadly, E. A. Rethinking the origin of primates by reconstructing their diel activity patterns using genetics and morphology. *Sci. Rep.* **7**, 11837 (2017).
16. Maor, R., Dayan, T., Ferguson-Gow, H. & Jones, K. E. Temporal niche expansion in mammals from a nocturnal ancestor after dinosaur extinction. *Nat. Ecol. Evol.* **1**, 1889–1895 (2017).
17. Wu, J., Yonezawa, T. & Kishino, H. Rates of molecular evolution suggest natural history of life history traits and a post-K-Pg nocturnal bottleneck of placentals. *Curr. Biol.* **27**, 3025–3033 (2017).
18. Shao, Y. et al. Phylogenomic analyses provide insights into primate evolution. *Science* **380**, 913–924 (2023).
19. Kawamura, S. Color vision diversity and significance in primates inferred from genetic and field studies. *Genes Genomics* **38**, 779–791 (2016).
20. Melin, A. D., Matsushita, Y., Moritz, G. L., Dominy, N. J. & Kawamura, S. Inferred L/M cone opsin polymorphism of ancestral tarsiers sheds dim light on the origin of anthropoid primates. *Proc. Biol. Sci.* **280**, 20130189 (2013).
21. Yokoyama, S. et al. Epistatic adaptive evolution of human color vision. *PLoS Genet.* **10**, e1004884 (2014).
22. Emerling, C. A., Huynh, H. T., Nguyen, M. A., Meredith, R. W. & Springer, M. S. Spectral shifts of mammalian ultraviolet-sensitive pigments (short wavelength-sensitive opsin 1) are associated with eye length and photic niche evolution. *Proc. Biol. Sci.* **282**, 20151817 (2015).
23. Morrow, J. M. et al. An experimental comparison of human and bovine rhodopsin provides insight into the molecular basis of retinal disease. *FEBS Lett.* **591**, 1720–1731 (2017).
24. Liu, Y. et al. Scotopic rod vision in tetrapods arose from multiple early adaptive shifts in the rate of retinal release. *Proc. Natl Acad. Sci. USA* **116**, 12627–12628 (2019).
25. Bickelmann, C. et al. The molecular origin and evolution of dim-light vision in mammals. *Evolution* **69**, 2995–3003 (2015).
26. Jacobs, G. H. Losses of functional opsin genes, short-wavelength cone photopigments, and color vision—a significant trend in the evolution of mammalian vision. *Vis. Neurosci.* **30**, 39–53 (2013).
27. Yokoyama, S., Tada, T., Liu, Y., Faggionato, D. & Altun, A. A simple method for studying the molecular mechanisms of ultraviolet and violet reception in vertebrates. *BMC Evol. Biol.* **16**, 64 (2016).
28. Yokoyama, S. Evolution of dim-light and color vision pigments. *Annu. Rev. Genomics Hum. Genet.* **9**, 259–282 (2008).

29. Ala-Laurila, P. et al. Visual cycle: dependence of retinol production and removal on photoproduct decay and cell morphology. *J. Gen. Physiol.* **128**, 153–169 (2006).
30. Dominy, N. J. & Melin, A. D. Liminal light and primate evolution. *Annu. Rev. Anthropol.* **49**, 257–276 (2020).
31. Melin, A. D., Moritz, G. L., Fosbury, R. A., Kawamura, S. & Dominy, N. J. Why aye-ayes see blue. *Am. J. Primatol.* **74**, 185–192 (2012).
32. Dungan, S. Z. & Chang, B. S. Epistatic interactions influence terrestrial–marine functional shifts in cetacean rhodopsin. *Proc. Biol. Sci.* **284**, 20162743 (2017).
33. Morrow, J. M. & Chang, B. S. Comparative mutagenesis studies of retinal release in light-activated zebrafish rhodopsin using fluorescence spectroscopy. *Biochemistry* **54**, 4507–4518 (2015).
34. Guo, J. et al. Convergent evolutionary shifts in rhodopsin retinal release explain shared opsin repertoires in monotremes and crocodilians. *Proc. Biol. Sci.* **290**, 20230530 (2023).
35. Castiglione, G. M. & Chang, B. S. Functional trade-offs and environmental variation shaped ancient trajectories in the evolution of dim-light vision. *eLife* **7**, e35957 (2018).
36. Davies, W. I., Collin, S. P. & Hunt, D. M. Molecular ecology and adaptation of visual photopigments in craniates. *Mol. Ecol.* **21**, 3121–3158 (2012).
37. Bender, B. J. et al. A practical guide to large-scale docking. *Nat. Protoc.* **16**, 4799–4832 (2021).
38. Lyu, J. et al. Ultra-large library docking for discovering new chemotypes. *Nature* **566**, 224–229 (2019).
39. Saito, H., Chi, Q., Zhuang, H., Matsunami, H. & Mainland, J. D. Odor coding by a mammalian receptor repertoire. *Sci. Signal.* **2**, ra9 (2009).
40. Nara, K., Saraiva, L. R., Ye, X. & Buck, L. B. A large-scale analysis of odor coding in the olfactory epithelium. *J. Neurosci.* **31**, 9179–9191 (2011).
41. Saraiva, L. R. et al. Combinatorial effects of odorants on mouse behavior. *Proc. Natl Acad. Sci. USA* **113**, E3300–E3306 (2016).
42. Harini, K. & Sowdhamini, R. Computational approaches for decoding select odorant–olfactory receptor interactions using mini-virtual screening. *PLoS ONE* **10**, e0131077 (2015).
43. Hallem, E. A. & Carlson, J. R. Coding of odors by a receptor repertoire. *Cell* **125**, 143–160 (2006).
44. Delbarco-Trillo, J., Burkert, B. A., Goodwin, T. E. & Drea, C. M. Night and day: the comparative study of strepsirrhine primates reveals socioecological and phylogenetic patterns in olfactory signals. *J. Evol. Biol.* **24**, 82–98 (2011).
45. Drea, C. M., Goodwin, T. E. & delBarco-Trillo, J. P-Mail: the information highway of nocturnal, but not diurnal or cathemeral, strepsirrhines. *Folia Primatol.* **90**, 422–438 (2019).
46. Drea, C. M. Design, delivery and perception of condition-dependent chemical signals in strepsirrhine primates: implications for human olfactory communication. *Philos. Trans. R. Soc. Lond. B* **375**, 20190264 (2020).
47. Carey, A. F., Wang, G., Su, C. Y., Zwiebel, L. J. & Carlson, J. R. Odorant reception in the malaria mosquito *Anopheles gambiae*. *Nature* **464**, 66–71 (2010).
48. Dominy, N. J. & Lucas, P. W. Ecological importance of trichromatic vision to primates. *Nature* **410**, 363–366 (2001).
49. Regan, B. C. et al. Fruits, foliage and the evolution of primate colour vision. *Philos. Trans. R. Soc. Lond. B* **356**, 229–283 (2001).
50. Barton, R. A. Visual specialization and brain evolution in primates. *Proc. Biol. Sci.* **265**, 1933–1937 (1998).
51. Barton, R. A., Purvis, A. & Harvey, P. H. Evolutionary radiation of visual and olfactory brain systems in primates, bats and insectivores. *Philos. Trans. R. Soc. Lond. B* **348**, 381–392 (1995).
52. DeCasien, A. R. & Higham, J. P. Primate mosaic brain evolution reflects selection on sensory and cognitive specialization. *Nat. Ecol. Evol.* **3**, 1483–1493 (2019).
53. Barton, R. A. Olfactory evolution and behavioral ecology in primates. *Am. J. Primatol.* **68**, 545–558 (2006).
54. Ross, C. F. Allometric and functional influences on primate orbit orientation and the origins of the Anthropoidea. *J. Hum. Evol.* **29**, 201–227 (1995).
55. Kaas, J. H., Huerta, M. F., Weber, J. T. & Harting, J. K. Patterns of retinal terminations and laminar organization of the lateral geniculate nucleus of primates. *J. Comp. Neurol.* **182**, 517–553 (1978).
56. Casagrande, V. A., Khaytin, I. & Boyd, J. in *The Evolution of Primate Nervous Systems* (eds Kaas, J. H. & Preuss, T. M.) 87–108 (Springer, 2007).
57. Heritage, S. Modeling olfactory bulb evolution through primate phylogeny. *PLoS ONE* **9**, e113904 (2014).
58. Gilad, Y., Przeworski, M. & Lancet, D. Loss of olfactory receptor genes coincides with the acquisition of full trichromatic vision in primates. *PLoS Biol.* **2**, E5 (2004).
59. Garrett, E. C. & Steiper, M. E. Strong links between genomic and anatomical diversity in both mammalian olfactory chemosensory systems. *Proc. Biol. Sci.* **281**, 20132828 (2014).
60. Webb, D. M., Cortés-Ortiz, L. & Zhang, J. Genetic evidence for the coexistence of pheromone perception and full trichromatic vision in howler monkeys. *Mol. Biol. Evol.* **21**, 697–704 (2004).
61. Garrett, E. C. *Was There a Sensory Trade-off in Primate Evolution? The Vomeronasal Groove as a Means of Understanding the Vomeronasal System in the Fossil Record*. PhD thesis, City Univ. of New York (2015).
62. Wysocki, C. J., Yamazaki, K., Curran, M., Wysocki, L. M. & Beauchamp, G. K. Mice (*Mus musculus*) lacking a vomeronasal organ can discriminate MHC-determined odortypes. *Horm. Behav.* **46**, 241–246 (2004).
63. Spehr, M. et al. Essential role of the main olfactory system in social recognition of major histocompatibility complex peptide ligands. *J. Neurosci.* **26**, 1961–1970 (2006).
64. Setchell, J. M. et al. Chemical composition of scent-gland secretions in an Old World monkey (*Mandrillus sphinx*): influence of sex, male status, and individual identity. *Chem. Senses* **35**, 205–220 (2010).
65. Lazaro-Perea, C., Snowdon, C. T. & de Fátima Arruda, M. Scent-marking behavior in wild groups of common marmosets (*Callithrix jacchus*). *Behav. Ecol. Sociobiol.* **46**, 313–324 (1999).
66. Geissmann, T. & Hulftegger, A. *Olfactory Communication in Gibbons* (Université Louis Pasteur, 1994).
67. Alport, L. J. Comparative analysis of the role of olfaction and the neocortex in primate intrasexual competition. *Anat. Rec. A* **281**, 1182–1189 (2004).
68. Fortes-Marco, L., Lanuza, E. & Martinez-Garcia, F. Of pheromones and kairomones: what receptors mediate innate emotional responses? *Anat. Rec.* **296**, 1346–1363 (2013).
69. Preuss, T. M. & Wise, S. P. Evolution of prefrontal cortex. *Neuropsychopharmacology* **47**, 3–19 (2022).
70. Li, M. L. et al. Functional genomics analysis reveals the evolutionary adaptation and demographic history of pygmy lorises. *Proc. Natl Acad. Sci. USA* **119**, e2123030119 (2022).
71. Kumar, S., Stecher, G., Li, M., Knyaz, C. & Tamura, K. MEGA X: molecular evolutionary genetics analysis across computing platforms. *Mol. Biol. Evol.* **35**, 1547–1549 (2018).
72. Darriba, D., Taboada, G. L., Doallo, R. & Posada, D. ProtTest 3: fast selection of best-fit models of protein evolution. *Bioinformatics* **27**, 1164–1165 (2011).
73. Yang, Z. PAML 4: phylogenetic analysis by maximum likelihood. *Mol. Biol. Evol.* **24**, 1586–1591 (2007).

74. Fabre, P. H., Rodrigues, A. & Douzery, E. J. Patterns of macroevolution among primates inferred from a supermatrix of mitochondrial and nuclear DNA. *Mol. Phylogenet. Evol.* **53**, 808–825 (2009).
75. Meredith, R. W. et al. Impacts of the Cretaceous terrestrial revolution and KPg extinction on mammal diversification. *Science* **334**, 521–524 (2011).
76. Upham, N. S., Esselstyn, J. A. & Jetz, W. Inferring the mammal tree: species-level sets of phylogenies for questions in ecology, evolution, and conservation. *PLoS Biol.* **17**, e3000494 (2019).
77. Maddison, W. P. & Maddison, D. R. Mesquite: a modular system for evolutionary analysis. Version 3.61 (2019).
78. Eick, G. N., Bridgham, J. T., Anderson, D. P., Harms, M. J. & Thornton, J. W. Robustness of reconstructed ancestral protein functions to statistical uncertainty. *Mol. Biol. Evol.* **34**, 247–261 (2017).
79. Yokoyama, S. Phylogenetic analysis and experimental approaches to study color vision in vertebrates. *Methods Enzymol.* **315**, 312–325 (2000).
80. Xia, Y. et al. Convergent phenotypic evolution of rhodopsin for dim-light sensing across deep-diving vertebrates. *Mol. Biol. Evol.* **38**, 5726–5734 (2021).
81. Beichman, A. C. et al. Aquatic adaptation and depleted diversity: a deep dive into the genomes of the sea otter and giant otter. *Mol. Biol. Evol.* **36**, 2631–2655 (2019).
82. Niimura, Y., Matsui, A. & Touhara, K. Extreme expansion of the olfactory receptor gene repertoire in African elephants and evolutionary dynamics of orthologous gene groups in 13 placental mammals. *Genome Res.* **24**, 1485–1496 (2014).
83. Yang, J. et al. The I-TASSER Suite: protein structure and function prediction. *Nat. Methods* **12**, 7–8 (2015).
84. Phillips, J. C. et al. Scalable molecular dynamics on CPU and GPU architectures with NAMD. *J. Chem. Phys.* **153**, 044130 (2020).
85. Huang, J. et al. CHARMM36m: an improved force field for folded and intrinsically disordered proteins. *Nat. Methods* **14**, 71–73 (2017).
86. Yang, J., Roy, A. & Zhang, Y. Protein–ligand binding site recognition using complementary binding-specific substructure comparison and sequence profile alignment. *Bioinformatics* **29**, 2588–2595 (2013).
87. Zheng, L. et al. MoDAFold: a strategy for predicting the structure of missense mutant protein based on AlphaFold2 and molecular dynamics. *Brief. Bioinform.* **25**, bbae006 (2024).
88. Billesbølle, C. B. et al. Structural basis of odorant recognition by a human odorant receptor. *Nature* **615**, 742–749 (2023).
89. Zhang, J., Yang, J., Jang, R. & Zhang, Y. GPCR-I-TASSER: a hybrid approach to G protein-coupled receptor structure modeling and the application to the human genome. *Structure* **23**, 1538–1549 (2015).
90. Kim, S. et al. PubChem in 2021: new data content and improved web interfaces. *Nucleic Acids Res.* **49**, D1388–D1395 (2021).
91. Sushko, I. et al. Online chemical modeling environment (OCHEM): web platform for data storage, model development and publishing of chemical information. *J. Comput. Aided Mol. Des.* **25**, 533–554 (2011).
92. Cao, Y., Charisi, A., Cheng, L., Jiang, T. & Girke, T. ChemmineR: a compound mining framework for R. *Bioinformatics* **24**, 1733–1734 (2008).
93. Haddad, R. et al. A metric for odorant comparison. *Nat. Methods* **5**, 425–429 (2008).
94. van der Maaten, L. & Hinton, G. Visualizing high-dimensional data using t-SNE. *J. Mach. Learn. Res.* **9**, 2579–2605 (2008).
95. Trott, O. & Olson, A. J. AutoDock Vina: improving the speed and accuracy of docking with a new scoring function, efficient optimization, and multithreading. *J. Comput. Chem.* **31**, 455–461 (2010).
96. Galili, T., O'Callaghan, A., Sidi, J. & Sievert, C. heatmaply: an R package for creating interactive cluster heatmaps for online publishing. *Bioinformatics* **34**, 1600–1602 (2018).
97. Lill, M. A. & Danielson, M. L. Computer-aided drug design platform using PyMOL. *J. Comput. Aided Mol. Des.* **25**, 13–19 (2011).
98. Fu, L., Niu, B., Zhu, Z., Wu, S. & Li, W. CD-HIT: accelerated for clustering the next-generation sequencing data. *Bioinformatics* **28**, 3150–3152 (2012).
99. Baud, O. et al. Exchanging ligand-binding specificity between a pair of mouse olfactory receptor paralogs reveals odorant recognition principles. *Sci. Rep.* **5**, 14948 (2015).
100. Teşileanu, T., Cocco, S., Monasson, R. & Balasubramanian, V. Adaptation of olfactory receptor abundances for efficient coding. *eLife* **8**, e39279 (2019).
101. DeCasien, A. R., Williams, S. A. & Higham, J. P. Primate brain size is predicted by diet but not sociality. *Nat. Ecol. Evol.* **1**, 112 (2017).
102. Young, J. M., Massa, H. F., Hsu, L. & Trask, B. J. Extreme variability among mammalian V1R gene families. *Genome Res.* **20**, 10–18 (2010).
103. Revell, L. J. phytools: an R package for phylogenetic comparative biology (and other things). *Methods Ecol. Evol.* **3**, 217–223 (2012).
104. Orme, D. et al. The caper package: comparative analysis of phylogenetics and evolution in R. R package version 5 (2013).
105. Arnold, C., Matthews, L. J. & Nunn, C. L. The 10kTrees website: a new online resource for primate phylogeny. *Evol. Anthropol.* **19**, 114–118 (2010).

Acknowledgements

We thank W. J. Murphy for providing valuable comments on earlier versions of this manuscript, R. Crouch from Medical University of South Carolina and L. Neuhold from National Eye Institute, NIH for 11-*cis*-retinal, H. Jing from Shaanxi Normal University for technical support and M. dos Reis from Queen Mary, University of London, for useful discussions about ancestral sequence reconstruction. We also thank the National Research Facility for Phenotypic & Genetic Analysis of Model Animals (Primate Facility) (https://cstr.cn/31137.02.NPRC) for providing technical support. This work was funded by the National Natural Science Foundation of China grant nos. 32270462 (Y.L.), 32470445 (G.L.), 32270525 (H.L.) and 31822048 (D.-D.W.), the Natural Science Basic Research Programme of Shaanxi grant nos. 2021JM-197 (Y.L.), 2020JM-280 (G.L.) and 2021JM-053 (H.L.), the Fundamental Research Funds for the Central Universities grant nos. GK202102006 (Y.L.), GK201902008 (G.L.), 2020TS050 (H.C.), the Strategic Priority Research Programme of the Chinese Academy of Sciences grant no. XDPB17 (D.-D.W.), Yunnan Provincial Science and Technology Department grant no. 202305AH340006 (D.-D.W.), National Sciences and Engineering Research Council of Canada grant no. RGPIN-2017-03782 (A.D.M.), Canada Research Chairs programme no. 950-231257 (A.D.M.) and were also supported in part by the Intramural Research Programme of the NIH (National Institute of Mental Health and National Institute on Aging) (A.R.D.).

Author contributions

Y.L., H.L., G.L. and D.-D.W. designed and supervised the research. H.C., A.D.M., Y.L., Y. Cui, X.G., Y. Zhan, N.L., J.G. and Z.X. performed evolutionary analyses and experimental assays for visual pigments. H.L., G.L., J. Wan, S.W., Y. Zhang, L.Z., J. Williamson, T.Z., Q.L., W.H., Y. Cao, J.Y., J.Z., Y.S., J. Wang and W.C. carried out functional modelling analyses for ORs. A.R.D. conducted integrative analyses of genetic, sensory and neuroanatomical data. G.L., Y.L., A.D.M., S.J.R., A.R.D., H.L., D.-D.W., H.C., S.S., X.L., X.Q. and G.Z. wrote the paper with comments from all listed authors.

Competing interests
The authors declare no competing interests.

Additional information
Supplementary information The online version contains supplementary material available at https://doi.org/10.1038/s41559-025-02651-5.

Correspondence and requests for materials should be addressed to Dong-Dong Wu, Yang Liu, Huimeng Lu or Gang Li.

Peer review information *Nature Ecology & Evolution* thanks Robert Barton, Robert Meredith, Yoshihito Niimura and the other, anonymous, reviewer(s) for their contribution to the peer review of this work.

[1]College of Life Sciences, Shaanxi Normal University, Xi'an, China. [2]School of Life Sciences, Northwestern Polytechnical University, Xi'an, China. [3]Department of Anthropology and Archaeology, University of Calgary, Calgary, Alberta, Canada. [4]Department of Medical Genetics, University of Calgary, Calgary, Alberta, Canada. [5]Alberta Children's Hospital Research Institute, University of Calgary, Calgary, Alberta, Canada. [6]Computational and Evolutionary Neurogenomics Unit, National Institute on Aging, Bethesda, MD, USA. [7]College of Animal Science and Veterinary Medicine, Shenyang Agricultural University, Shenyang, China. [8]QinLing-Bashan Mountains Bioresources Comprehensive Development C. I. C., School of Bioscience and Engineering, Shaanxi University of Technology, Hanzhong, China. [9]School of Biological and Behavioural Sciences, Queen Mary, University of London, London, UK. [10]State Key Laboratory of Genetic Evolution & Animal Models, Kunming Natural History Museum of Zoology, Kunming Institute of Zoology, Chinese Academy of Sciences, Kunming, China. [11]Guangzhou Zoo & Guangzhou Wildlife Research Center, Guangzhou, China. [12]School of Life Sciences, Westlake University, Hangzhou, China. [13]Shaanxi Key Laboratory for Animal Conservation, College of Life Sciences, Northwest University, Xi'an, China. [14]BGI-Shenzhen, Shenzhen, China. [15]Villum Center for Biodiversity Genomics, Section for Ecology and Evolution, Department of Biology, University of Copenhagen, Copenhagen, Denmark. [16]National Resource Center for Non-Human Primates, Kunming Primate Research Center, and National Research Facility for Phenotypic & Genetic Analysis of Model Animals (Primate Facility), Kunming Institute of Zoology, Chinese Academy of Sciences, Kunming, China. [17]Center for Excellence in Animal Evolution and Genetics, Chinese Academy of Sciences, Kunming, China. [18]These authors contributed equally: Hai Chi, Jiahui Wan, Amanda D. Melin. ✉e-mail: wudongdong@mail.kiz.ac.cn; yliu@snnu.edu.cn; luhuimeng@nwpu.edu.cn; gli@snnu.edu.cn

nature portfolio

Corresponding author(s): Gang Li, Hui-Meng Lu, Yang Liu and Dong-Dong Wu

Last updated by author(s): Jan 23, 2025

Reporting Summary

Nature Portfolio wishes to improve the reproducibility of the work that we publish. This form provides structure for consistency and transparency in reporting. For further information on Nature Portfolio policies, see our Editorial Policies and the Editorial Policy Checklist.

Statistics

For all statistical analyses, confirm that the following items are present in the figure legend, table legend, main text, or Methods section.

n/a	Confirmed	
☐	☒	The exact sample size (*n*) for each experimental group/condition, given as a discrete number and unit of measurement
☐	☒	A statement on whether measurements were taken from distinct samples or whether the same sample was measured repeatedly
☐	☒	The statistical test(s) used AND whether they are one- or two-sided *Only common tests should be described solely by name; describe more complex techniques in the Methods section.*
☒	☐	A description of all covariates tested
☐	☒	A description of any assumptions or corrections, such as tests of normality and adjustment for multiple comparisons
☐	☒	A full description of the statistical parameters including central tendency (e.g. means) or other basic estimates (e.g. regression coefficient) AND variation (e.g. standard deviation) or associated estimates of uncertainty (e.g. confidence intervals)
☐	☒	For null hypothesis testing, the test statistic (e.g. *F*, *t*, *r*) with confidence intervals, effect sizes, degrees of freedom and *P* value noted *Give P values as exact values whenever suitable.*
☒	☐	For Bayesian analysis, information on the choice of priors and Markov chain Monte Carlo settings
☒	☐	For hierarchical and complex designs, identification of the appropriate level for tests and full reporting of outcomes
☐	☒	Estimates of effect sizes (e.g. Cohen's *d*, Pearson's *r*), indicating how they were calculated

Our web collection on statistics for biologists contains articles on many of the points above.

Software and code

Policy information about availability of computer code

Data collection	No softwares were used for Data collection.
Data analysis	BLAST, ClustalW, MEGA X (v10.1.81), ProtTest 3, PAML 4, MUSCLE (v3.8.31), I-TASSER (v5.1), NAMD (v3.0a), COACH, AutoDock Vina (v1.12), R (v4.03), PyMOL (v2.3.0), CD-HIT (v4.8.1), Mesquite 3. Code to run the analyses are available at https://github.com/GanglabSnnu/OR_identify

For manuscripts utilizing custom algorithms or software that are central to the research but not yet described in published literature, software must be made available to editors and reviewers. We strongly encourage code deposition in a community repository (e.g. GitHub). See the Nature Portfolio guidelines for submitting code & software for further information.

Data

Policy information about availability of data

All manuscripts must include a data availability statement. This statement should provide the following information, where applicable:

- Accession codes, unique identifiers, or web links for publicly available datasets
- A description of any restrictions on data availability
- For clinical datasets or third party data, please ensure that the statement adheres to our policy

The opsin gene sequences are available in public databases, the NCBI (www.ncbi.nlm.nih.gov). All phenotypic data of visual pigments analyzed here are included in this article. Figure 1 and also Supplementary Figures S5-7 are associated with raw data (see Supplementary Data). The OR gene sequences are submitted with this article as a section of the supplementary material.

Research involving human participants, their data, or biological material

Policy information about studies with human participants or human data. See also policy information about sex, gender (identity/presentation), and sexual orientation and race, ethnicity and racism.

Reporting on sex and gender	No human participants or human data were involved in this research
Reporting on race, ethnicity, or other socially relevant groupings	No human participants or human data were involved in this research
Population characteristics	No human participants or human data were involved in this research
Recruitment	No human participants or human data were involved in this research
Ethics oversight	No human participants or human data were involved in this research

Note that full information on the approval of the study protocol must also be provided in the manuscript.

Field-specific reporting

Please select the one below that is the best fit for your research. If you are not sure, read the appropriate sections before making your selection.

☐ Life sciences ☐ Behavioural & social sciences ☒ Ecological, evolutionary & environmental sciences

For a reference copy of the document with all sections, see nature.com/documents/nr-reporting-summary-flat.pdf

Ecological, evolutionary & environmental sciences study design

All studies must disclose on these points even when the disclosure is negative.

Study description	We conduct comprehensive functional genomic analyses based on genomes of 50 species from 14 families representing all major primate lineages, including newly-published, high-quality genome data from 27 primate species. We present new data on: 1) visual pigment gene sequences and functional assays of color sensitivity and dim-light adaptation; 2) olfactory receptor gene sequences and the first comprehensive and systematic models of olfactory receptor tuning; and 3) we integrate these data with published genetic, sensory, and neuroanatomical data to examine patterns of correlated evolution. Overall, we reconstruct the most comprehensive assessment of phenotypic evolution of vision and olfaction in modern and ancient primates.
Research sample	Based on published gene sequences for evolutionary analyses.
Sampling strategy	Published gene sequences were chosen to encompass major primate lineages, with appropriate inclusion of outgroups.
Data collection	We used a newly published dataset of long-read, high coverage genomes from the primate genomes project, along with previously published reference genomes of primates. Altogether, the genomes of 50 species from 14 families representing all major primate lineages were analysed. Hominidae (Homo sapiens, Gorilla gorilla, Pan paniscus, Pan troglodytes, Pongo abelii, Pongo pygmaeus), Hylobatidae (Hoolock leuconedys, Hylobates pileatus, Nomascus siki, Symphalangus syndactylus), Cercopithecidae (Cercocebus atys, Cercopithecus albogularis, Cercopithecus mona, Chlorocebus aethiops, Chlorocebus sabaeus, Colobus angolensis, Colobus guereza, Erythrocebus patas, Lophocebus aterrimus, Macaca assamensis, Macaca mulatta, Macaca nemestrina, Macaca silenus, Mandrillus leucophaeus, Mandrillus sphinx, Papio anubis, Papio hamadryas, Piliocolobus tephrosceles, Pygathrix nigripes, Rhinopithecus roxellana, Rhinopithecus strykeri, Theropithecus gelada, Trachypithecus phayrei), Callitrichidae (Callithrix jacchus, Saguinus midas), Aotidae (Aotus nancymaae), Cebidae (Cebus albifrons, Sapajus apella), Atelidae (Ateles geoffroyi), Pitheciidae (Pithecia pithecia), Tarsiidae (Tarsius syrichta), Daubentoniidae (Daubentonia madagascariensis), Cheirogaleidae (Microcebus murinus), Lemuridae (Prolemur simus, Lemur catta), Lorisidae (Loris tardigradus, Nycticebus bengalensis, Nycticebus pygmaeus), Galagidae (Galago moholi, Otolemur garnettii). The published primate genomic sequences were collected from online repositories for gene searching. Moreover, additional SWS1 and RH1 sequences from primates (57 SWS1 and 49 RH1) and outgroups were also obtained from public database. Phenotype data for synthesized proteins were obtained in the lab.
Timing and spatial scale	The data collection period is from 2020 to 2023
Data exclusions	No data were excluded.
Reproducibility	Recordings were taken from 3-7 technical replicates.
Randomization	The primate genomic data used in this research were obtained from the public NCBI database. The genomic data with the best assembling quality were involved in this research for the sensory gene searching.
Blinding	no blinding was needed in this research

Did the study involve field work? ☐ Yes ☒ No

Reporting for specific materials, systems and methods

We require information from authors about some types of materials, experimental systems and methods used in many studies. Here, indicate whether each material, system or method listed is relevant to your study. If you are not sure if a list item applies to your research, read the appropriate section before selecting a response.

Materials & experimental systems

n/a	Involved in the study
☐	☒ Antibodies
☐	☒ Eukaryotic cell lines
☒	☐ Palaeontology and archaeology
☒	☐ Animals and other organisms
☒	☐ Clinical data
☒	☐ Dual use research of concern
☒	☐ Plants

Methods

n/a	Involved in the study
☒	☐ ChIP-seq
☒	☐ Flow cytometry
☒	☐ MRI-based neuroimaging

Antibodies

Antibodies used: RHO 1D4 Antibody (0.1ug/ul) (University of British Columbia).

Validation: The antibody purchased from the University of British Columbia (https://ubc.flintbox.com/technologies/0f1ef64b-fa5d-4a58-9003-3e01f6f672a6).

Eukaryotic cell lines

Policy information about cell lines and Sex and Gender in Research

Cell line source(s): HEK293T (ATCC).

Authentication: The cell line was authenticated by genotyping.

Mycoplasma contamination: The cell line was tested negative for mycoplasma.

Commonly misidentified lines (See ICLAC register): N/A

Plants

Seed stocks: N/A

Novel plant genotypes: N/A

Authentication: N/A